Iron overload enhances human mesenchymal stromal cell growth and hampers matrix calcification☆

Adriana Borriello [a,*], Ilaria Caldarelli [a], Maria Carmela Speranza [a], Saverio Scianguetta [b], Annunziata Tramontano [a], Debora Bencivenga [a], Emanuela Stampone [a], Aide Negri [c], Bruno Nobili [b], Franco Locatelli [d], Silverio Perrotta [b], Adriana Oliva [a], Fulvio Della Ragione [a,*]

[a] Department of Biochemistry, Biophysics and General Pathology, Second University of Naples, 80138 Naples, Italy
[b] Dipartimento della Donna, del Bambino e di Chirurgia Generale e Specialistica, Second University of Naples, 80138 Naples, Italy
[c] Dipartimento di Scienze Biomediche Sperimentali e Cliniche, Università degli Studi di Firenze, 50134 Firenze, Italy
[d] Department of Pediatric Hematology and Oncology, Bambino Gesù Children's Hospital, IRCCS, Rome, University of Pavia, Italy

ARTICLE INFO

ABSTRACT

Background: Iron overload syndromes include a wide range of diseases frequently associated with increased morbidity and mortality. Several organs are affected in patients with iron overload including liver, heart, joints, endocrine glands, and pancreas. Moreover, severe bone and hemopoietic tissue alterations are observed. Because of the role of bone marrow mesenchymal stromal cells (BM-MSCs) in bone turnover and hematopoiesis, iron effects on primary BM-MSCs cultures were evaluated.
Methods: Primary human BM-MSCs cultures were prepared and the effects of iron on their proliferation and differentiation were characterized by biochemical analyses and functional approaches.
Results: Addition of iron to the culture medium strongly increased BM-MSCs proliferation and induced their accelerated S phase entry. Iron enters BM-MSCs through both transferrin-dependent and transferrin-independent mechanisms, inducing the accumulation of cyclins E and A, the decrease of p27^{Kip1}, and the activation of MAPK pathway. Conversely, neither apoptotic signs nor up-regulation of reactive oxygen species were observed. Iron inhibited both differentiation of BM-MSCs into osteoblasts and *in vitro* matrix calcification. These effects result from the merging of inhibitory activities on BM-MSCs osteoblastic commitment and on the ordered matrix calcification process.
Conclusions: We demonstrated that BM-MSCs are a target of iron overload. Iron accelerates BM-MSCs proliferation and affects BM-MSCs osteoblastic commitment, hampering matrix calcification.
General Significance: Our study reports, for the first time, that iron, at concentration found in overloaded patient sera, stimulates the growth of BM-MSCs, the BM multipotent stromal cell component. Moreover, iron modulates the physiological differentiation of these cells, affecting bone turnover and remodeling.

© 2016 Elsevier B.V. All rights reserved.

1. Introduction

Iron overload describes a condition in which total body iron stores are increased, with or without organ dysfunction [1,2]. Iron homeostasis is associated with a complex feedback mechanism between body requirements and intestinal absorption. Particularly, because of the absence of physiological mechanism(s) for active iron excretion, human iron levels are controlled by modulation of intestinal uptake and unceasing metabolic recycling [1,2]. The diseases that cause iron overload are classified as primary or secondary, depending on the etiology. Inherited primary iron overload syndromes mainly include hemochromatosis, caused by alterations of different genes, such as *HFE*, *hemojuvelin*, *hepcidin*, *transferrin receptor type II*, and *ferroportin* genes [3,4]. Secondary iron overload syndromes are due to hematological

disorders, chronic liver diseases, porphyria cutanea tarda, and other diseases [5]. Particularly, five major types of hematological disorders result in iron overload: (a) thalassemia syndromes (thalassemia major, non-transfusion-dependent thalassemia, and sickle cell diseases); (b) congenital dyserythropoietic anemias; (c) transfusion-dependent anemias including pyruvate kinase deficiency, Fanconi anemia, Diamond–Blackfan anemia, and aplastic anemia; (d) sideroblastic anemias, and (e) myelodysplastic syndrome. Thalassemic syndromes are, by far, the most common causes of ineffective erythropoiesis and secondary iron overload.

Several organs are affected by iron overload including liver, heart, joints, skin, and endocrine glands [6], resulting in cirrhosis, cardiomyopathy, arthropathy, diabetes mellitus, hypopituitarism, hypothyroidism, and hypogonadism [6]. Additionally, important bone alterations, such as osteoporosis and fractures, have been documented in hematological iron overload diseases [7–10] and in animal models [11,12]. In particular, iron overloaded mice show changes in bone composition and trabecular and cortical thinning of bone accompanied by increased bone resorption [12]. A further target of iron toxicity is the erythropoietic process. Indeed, treatment with iron chelating agents results in improved hemoglobin levels and reduced red blood cell transfusion requirements, suggesting that iron overload negatively affects erythropoiesis [13,14]. However, the cellular and molecular bases of these phenomena are not completely unraveled. Iron overload inhibits *in vitro* burst-forming unit colony formation and erythroblastic differentiation of both murine and human hematopoietic progenitors [14,15]; some experiments suggested a role for reactive oxygen species (ROS) upregulation and a decrease in Bcl-2 (an antiapoptotic protein), but no general conclusions have been reached [14,15].

Mesenchymal stromal cells (MSCs) are multipotent cells that can differentiate into all mesenchymal lineages, including mostly osteoblasts and adipocytes [16]. So far, although various sources have been identified, adipose tissue and bone marrow (BM) represent the major MSC sources [17,18]. Recent studies, however, have identified fundamental differences between adipose tissue MSCs and BM-MSCs, in terms of phenotypic properties [19]. Human BM-MSCs (hBM-MSCs) are crucial in bone physiology, because they play at least three major roles. One is linked to their differentiation into osteoblasts and, in turn, to the general control of bone turnover and fracture healing [20]. The second major function of hBM-MSCs is the participation into the hematopoietic niche organization and thus in the blood cell origin process [21,22]. In the niche microenvironment, BM-MSCs play a key role in hematopoietic stem cell commitment, mobilization, and exit from BM. In turn, the interaction with several different cell types, such as fibroblasts, endothelial cells, osteoblasts, osteoclasts, adipocytes, and immune cells, profoundly affects the BM-MSC phenotype [21,22]. Finally, BM-MSCs display immunomodulatory functions directed against all the cells involved in both adaptive and innate immune response. Thanks to these latter properties, MSCs contribute to maintenance of tissue homeostasis and may have a therapeutic role in immune-related disorders [23]. Thus, because of the role of hBM-MSCs in hemopoiesis and bone metabolism and the negative influence of iron overload on erythropoiesis and bone structure, we decided to investigate the effect of iron on the proliferation and osteoblastic differentiation of hBM-MSCs. So far, scarce information is available on the effect of iron on osteoblasts [24–27]. The few published studies were based on established osteoblast cell lines and/or osteoblasts of non-human origin [24–27]. No detailed studies are available on primary cultures of hBM-MSCs at early passages, a condition necessary to maintain the original phenotype.

In this study, we report the effects of iron (at concentrations ranging from physiological to those observed in iron overload diseases) on the proliferation and differentiation of primary cultures of hBM-MSCs. The results obtained demonstrate, for the first time, that the addition of iron to the culture medium strongly stimulates hBM-MSCs growth. The increase in the proliferation rate corresponds to a diminished capability of the cells to differentiate toward osteoblasts, produce collagen, and calcify the extracellular matrix. Moreover, we showed that iron overload results in a significant accumulation of iron in hBM-MSCs, suggesting that these cells are key targets in iron overload syndromes.

2. Materials and methods

2.1. Preparation and characterization of hBM-MSCs

hBM-MSCs were obtained from heparinized human BM samples of healthy volunteers. Preparation, propagation, and phenotypic characterization of hBM-MSCs cultures were performed as described [28,29]. Only second-third passage cultures were used in the reported experiments. The study was approved by the Medical Ethics Committee of the Second University of Naples and performed in accordance with the Declaration of Helsinki. Written informed consent was obtained from all subjects prior to the participation in the study.

2.2. Evaluation of hBM-MSC proliferation rate

Iron was added to the cells as Ferric Ammonium Citrate, FAC (Sigma Chemical Company, St. Louis, MO, USA). All the culture media and supplements were from Invitrogen Life Technology, Carlsbed, CA, USA. Effects of FAC on cell growth were evaluated on cells seeded at low density ($5–10 \times 10^3$ cells/cm^2) the day before the treatment and cultured in standard medium [SM: Dulbecco's Modified Eagle's Medium, DMEM, 10% FCS (fetal calf serum), 100 units/ml penicillin, 100 μg/ml streptomycin, 2.5 μg/ml fungizone]. In control cultures, Sodium Ammonium Citrate, SAC (Sigma) was added. Images of cells were taken under an Axiovert-10 Zeiss microscope in bright field. Proliferation rate was evaluated by direct cell counting using a Burker chamber. The cell cycle distribution was evaluated as described [29] by propidium iodide staining and flow cytometric analysis using a FACScalibur (Becton Dickinson, CA, USA) and calculated from 30.000 to 40.000 events using ModFit LTTM software (Becton Dickinson, CA, USA).

2.3. Evaluation of intracellular ROS levels

ROS production was determined using 2′,7′-dichlorofluorescein diacetate (DCF-DA, Sigma Chemical Company). hBM-MSCs, seeded the day before in 12-well culture plates at low density, were treated for 3 h with different concentrations of FAC, SAC, or 1 mM *tert*-butyl hydroperoxide (positive control). After washing, cells were incubated for 30 min with DCF-DA at 37 °C in 5% CO$_2$. Inside the cells, DCF-DA is de-esterified and turns to highly fluorescent 2′,7′-dichlorofluorescein upon oxidation by intracellular peroxides. Formation of oxidized DCF was monitored in cell lysates by fluorescence spectroscopy at excitation wavelength of 502 nm and emission wavelength of 523 nm. The ROS levels were expressed as RFU (relative fluorescent unit)/10^3 cells.

2.4. Osteoblastic differentiation methods

To evaluate the iron effect on MSCs osteogenesis, confluent cells (usually seeded at density of $4–5 \times 10^4$ cells/cm^2 in 6-well plates) were previously exposed to 7 days pre-treatment in SM plus 100 μM FAC or 100 μM SAC, as control. Both SM/FAC or SM/SAC media were added or not with 50 μg/ml L-ascorbic acid. After the iron upload, cells were rinsed, left for 1 day in fresh SM, and induced to osteogenic differentiation as follows. Cells were cultured in osteogenic medium (OM) (namely, SM plus 100 nM dexamethasone, 50 μg/ml L-ascorbic acid and 10 mM β-glycerophosphate) for 2–3 weeks, and monitored daily to identify signs of matrix mineralization. The effects of treatments on osteogenic differentiation were evaluated by analyzing specific markers of osteogenic phenotype, namely alkaline phosphatase (AP) activity, osteocalcin (OC) production and mineralization of the extracellular matrix.

2.4.1. Alkaline phosphatase activity assay

AP activity was assayed as follows. Cells were lysed in TBS (20 mM tris(hydroxymethyl)aminomethane/HCl, pH 7.4, 0.5 M NaCl) plus 0.25% Triton X-100, 0.5 mM phenylmethylsulfonyl fluoride and 0.5 mM dithiothreitol. After 30 min on ice, the cell lysates were centrifuged at $13,000 \times g$ for 10 min, and the supernatants were employed for evaluating AP activity. AP activity was determined by measuring the release of *para*-nitrophenol from disodium *para*-nitrophenyl phosphate (PNPP). The reaction mixture contained 0.1 M diethanolamine phosphate buffer, pH 10.5, 0.5 mM $MgCl_2$, 10 mM PNPP, and 10–30 µg of cell lysate in a final volume of 0.5 ml. After 30 min at 37 °C, the reaction was stopped by adding equal volume of 0.5 M NaOH. *Para*-nitrophenol levels were measured spectrophotometrically at a wavelength of 405 nm. One unit was defined as the amount of enzyme that hydrolyzes 1 nmol of PNPP/min under the reported conditions. AP protein levels were also evaluated by western blotting analysis.

2.4.2. Determination of osteocalcin synthesis and secretion in the medium

To evaluate OC synthesis, confluent hBM-MSC layers, treated under the investigated conditions, were cultured for further 48 h in a specific medium consisting of FCS-free Opti-MEM, 0.1% bovine serum albumin, and 100 nM 1,25-dihydroxycolecalciferol (active vitamin D3 form). The amount of the polypeptide secreted in the medium were determined by means of Osteocalcin human ELISA kit (Biosource International, Camarillo, CA, USA), following manufacturer's instructions. OC concentrations were obtained by interpolation from a standard calibration curve and normalized to the cell number or alternatively to the cell extract proteins (ng/mg proteins).

2.4.3. Evaluation of the extracellular matrix mineralization

Von Kossa, Alizarin Red Staining (ARS), and *o*-cresolphthalein complexone methods were employed to quantify the extracellular matrix mineralization.

The Von Kossa Method is able to reveal the phosphate (instead of the calcium) deposition into the extracellular matrix. Briefly, cells were fixed with 4% paraformaldehyde, washed three times with phosphate buffered solution (PBS, 37 mM NaCl, 2.7 mM KCl, 10 mM phosphate, pH 7.4), and incubated in a 1% silver nitrate solution in the dark for 30 min. Afterwards, plates were washed with distilled water and exposed to UV light for 10 min. The formed Ag_3PO_4 gives a dark-brown staining whose intensity is indicative of the extracellular mineralization. Both *o*-cresolphthalein complexone method and ARS were used to quantify the mineralization of the extracellular matrix. In the *o*-cresolphthalein complexone technique, cells were washed with PBS, scraped from the plates, transferred into 1.5-ml microcentrifuge tubes, and subjected to a decalcification reaction for 24 h in 0.6 N HCl ($2–3 \times 10^6$ cellule/ml) at room temperature. Then, the slurries were centrifuged at $15,000 \times g$ for 10 min and 500 µl of supernatants were transferred into new tubes: the calcium released in the supernatants was determined on a Aeroset Multichamber (Abbot Clinical Chemistry) by adding a color reagent substrate solution containing *o*-Cresolphthalein Complexone Arsenazo III [2,2′-(1,8-Dihydroxy-3,6-disulfonaphthylene-2,7-bisazo)bisbenzenearsonic acid]. In the final mixture, calcium in alkaline medium reacts with o-cresolphthalein complexone to form a purple colored complex whose absorbance at a wavelength of 660 nm is proportional to the calcium concentration. The corresponding calcium quantities were obtained by interpolation from a standard calibration curve and normalized for cell number (µg calcium/10^6 cells).

In the ARS method, cells were washed with PBS and fixed by incubation in 10% (v/v) formaldehyde at room temperature for 15 min. The monolayers were washed with distilled water and added with 1 ml of 40 mM Alizarin Red S (Sigma), pH 4.1. After 20 min incubation under gentle shaking, the unincorporated dye was discarded and the cells were washed with distilled water prior to obtaining images under microscopy or to proceeding to quantification. For staining quantification,

800 µl of a 10% acetic acid solution was added to each well. The monolayers were then scraped from the plates and transferred into 1.5-ml microcentrifuge tubes. After vortexing for 30 s, the slurries were overlaid with 500 µl mineral oil, heated to 85 °C for 10 min, transferred to ice for 5 min, and centrifuged at $20,000 \times g$ for 15 min. Then, 500 µl of the supernatants was moved to new tubes and added with 200 µl of 10% ammonium hydroxide to neutralize the acid. Aliquots (150 µl) of the supernatants were read in triplicate at 405 nm. ARS was expressed as absorbance/10^6 cells.

2.5. Hypoxia signaling pathway RT-PCR array

hBM-MSCs were seeded in 6-well plates at low density ($5–10 \times 10^3$ cells/cm^2). After 1 day, proliferating cells were treated with 100 µM FAC, 100 µM SAC, or 100 µM CoCl2 for 72 h. Total RNA was extracted from treated and control cells, using TRIzol reagent, according to manufacturer's instructions (Invitrogen) and resuspended in RNase-free water. cDNA was synthesized from 1 µg of RNA using RT^2 First Strand Kit (SABiosciences, QIAGEN) and analyzed using RT^2 Profiler PCR arrays specific for the Hypoxia Signaling Pathway (PAHS-032ZA-12) and the RT^2 SYBR green ROX qPCR master mix (SABiosciences, QIAGEN), according to manufacturer's instructions. The array consists of 84 genes known to be involved in the hypoxic response, cell differentiation, and metabolism, as well as 12 sequences to control for loading and cDNA quality (housekeeping genes, genomic DNA control, reverse transcription controls, and positive PCR controls). Amplification, data acquisition, and analysis curves were performed on ABI Prism 7900 HT Sequence Detection System (Applied Biosystems, Foster City, CA, USA).

Gene expression was defined from the threshold cycle (Ct), and relative expression levels were calculated using SA-Biosciences RT^2 Profiler PCR array analysis automated software (http://pcrdataanalysis. sabiosciences.com/pcr/arrayanalysis.php).

Quantitative PCR (qPCR) analyses were performed for evaluating the expression of *endothelin 1*, *carbonic anhydrase 9*, *TfR1*, and *angiopoietin-like protein 4*. The PCR conditions were described in [30] and the sequences of the employed primers are available upon request.

2.6. Reverse transcriptase-PCR (RT-PCR) assay

RT-PCR was mainly performed as reported [31]. The sequences of the primers employed for the analyzed transcripts (COL1A1, GAPDH) will be available upon request. After PCR reaction, the products were separated by electrophoresis on agarose gels and visualized as described previously [31]. Signals were quantified by analysis of the scanner band intensities using ImageJ64 software.

2.7. Cell lysates preparation and analysis

Total cell extracts were prepared as reported [29,31]. Nuclear and cytoplasmic extracts were prepared using NE-PER Nuclear and Cytoplasmic Extraction Reagents, furnished by Thermo Fisher Scientific (Rockford, IL, USA), following manufacturer's instructions. Immunoblotting analyses were carried as previously reported [31], employing several antibodies. Rabbit polyclonal antibodies against cyclin A (sc-751), Erk1/2 (K23, sc-94) HDAC1 (sc-7872), Collagen α2 Type I (sc-8786), and monoclonal antibodies against cyclin E (HE12, sc-247), human Collagen α2 Type I (H9, sc-376,350), phospho-Erk1/2 (K23, sc-7383) were from Santa Cruz Biotechnology, Inc. (Santa Cruz, CA, USA). Monoclonal antibodies (mAb) to $p27^{Kip1}$ were from BD Transduction Laboratories (Franklin Lakes, NJ, USA). Rabbit polyclonal anti-actin antibodies were furnished by Sigma. The anti-transferrin antiserum employed in the experiment evaluating iron entry mechanisms was sc-21011 (H-65, Santa Cruz Biotechnology). For collagen type I immunoblotting analysis, an equal number (1×10^6) of control and treated cells were recovered and resuspended in 250–500 µl of 0.5 M acetic acid. Pepsin was added to the suspensions at a final concentration of 350 µg/ml and left

overnight at 4 °C under gentle rocking, allowing the proteolytic digestion of the majority of the cellular proteins but collagen. Thereafter, samples were centrifuged at 15.000 ×g for 60 min and pellets were resuspended in 25–50 μl of SDS-PAGE loading buffer and analyzed by immunoblotting as usually. Immunoblotting signals were quantified by the analysis of scanner band intensities using ImageJ64 software.

To estimate intracellular iron and ferritin levels, equal numbers of cells (0.5–1×10^6) were collected by centrifugation and resuspended in lysis buffer. Alternatively, cell pellets were resuspended in cold water and cell lysis was obtained by three cycles of freezing and thawing. The lysates were then centrifuged at 15.000 ×g for 10 min. Iron and ferritin levels were estimated by means of commercially available kits, on a Roche Cobas C 501 system (F. Hoffmann–La Roche Ltd). Specifically, for intracellular iron determination, Iron Gen.2 reagent (Roche Diagnostics) was used and the obtained data were expressed as ng Fe/10^6 cells. For intracellular ferritin, a particle-enhanced immunoturbidimetric assay using a Tina-quant Ferritin Gen.4 (Roche Diagnostics) was employed. Data were expressed as ng ferritin/10^6 cells.

2.8. Statistical analysis

Experimental data were expressed as mean ± SD. GraphPad Prism 6 (GraphPad Software, La Jolla, CA, USA) was used for statistical analysis. Comparisons between treated samples and control were performed using Sample T test or ANOVA. *P* value <0.05 was considered to be significantly different.

3. Results

3.1. Effect of iron overload on MSCs proliferation

In our investigation, we exposed hBM-MSCs to FAC concentrations initially ranging from 20 to 200 μM (i.e. from 110 to 1100 μg/dl). FAC efficaciously mimics the so-called Non-Transferrin Bound Iron (NTBI) occurring in the plasma of iron overloaded patients [32]. The employed FAC interval spans from normal serum iron levels (from 50 to 180 μg/dL) to a concentration equivalent of six-fold the normal values. We did not test higher iron concentrations since they are not reached in iron overload diseases. The concentration of iron in the standard medium (DMEM plus 10% fetal bovine serum) was 3 ± 1 μM, accordingly to previous reports [25]. Thus, total iron concentration employed starts from about 23 μM and reaches 203 μM. To identify the effect of iron on hBM-MSC phenotype, cells were plated at low density and cultured for different time intervals in the presence of FAC (treated cells) or SAC (control cells). Initial microscopy evidence suggested that 100 μM iron enhances cell growth after 3 days (Fig. 1A). The histograms in Figs. 1B and 1C show the cell number of hBM-MSCs after incubation at various iron concentrations for 3 (Fig. 1B) or 7 days (Fig. 1C). The data reported were obtained for two different primary cell populations. Moreover, taking into consideration
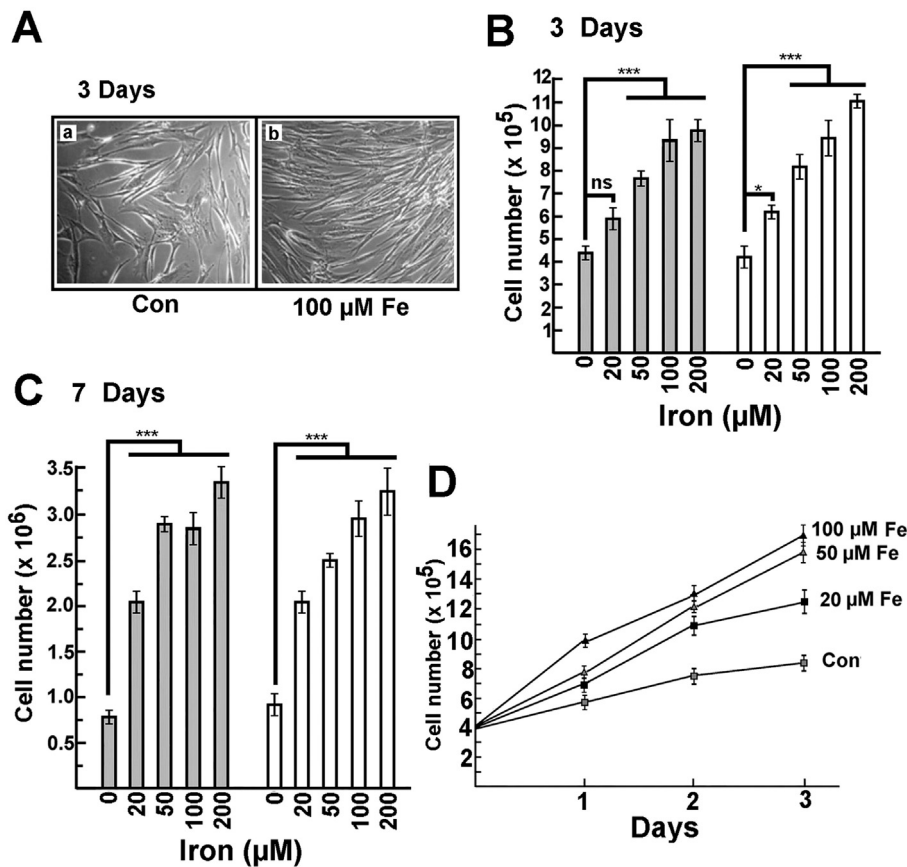

Fig. 1. Effect of iron on proliferation of hBM-MSCs. Panel *A*: Microphotographies of hBM-MSCs grown for 3 days without (a) or with (b) 100 μM iron. Panel *B*: Two different hBM-MSC populations (in gray and white, respectively) were grown for 3 days at different iron concentrations. Then, cell number was evaluated by direct counting. Each population was analyzed in three independent experiments; each experiment was performed in duplicate. The data reported represent the mean values ± S.D. ns, not significant, *P < 0.05, ***P < 0.001 compared to 0 μM iron. Panel *C*: Two different hBM-MSC populations (in gray and white, respectively) were grown for 7 days with different amounts of iron. Subsequently, cell number was evaluated by direct counting. Each population was analyzed in three independent experiments; each experiment was performed in duplicate. The data reported represent the mean values ± S.D. ***P < 0.001 compared to 0 μM iron. Panel *D*: hBM-MSCs were grown up to 3 days without (Con) or with 20, 50, or 100 μM iron. At 1-day intervals, the cell number was evaluated by direct counting. The data reported represent the mean values ± S.D. of three independent experiments; each experiment was performed in duplicate.

all the independent cell preparations investigated (twenty), we calculated an overall iron-dependent increase of cell number of about 1.8-folds after 3 days and 3.6-folds after 7 days at 50 μM iron treatment. We also evaluated the effect of iron on cell proliferation in the time window of the initial 3 days of treatment (Fig. 1D). The results clearly demonstrated that iron addition accelerates cell growth precociously and at low concentrations (20–50 μM). Following these observations, a FAC interval from 20 to 100 μM was used in the majority of the subsequent experiments. This range includes iron concentrations reached in human iron overload-associated diseases. Iron and ferritin levels were determined in control and treated cells. As shown in Fig. 2A, the increase in intracellular iron was time- and concentration-dependent. Accordingly, ferritin accumulation was observed, showing that an accelerated ferritin transcript translation occurs even after 24 h of incubation (Fig. 2B). We also asked whether hBM-MSC iron uptake needed binding to transferrin (Tf), followed by endocytosis of the iron-charged holotransferrin/Tf receptor (TfR) complex. Thus, 100 μg of rabbit anti-transferrin antiserum was added to the medium (containing 5% FCS) of both control and iron-treated cells. After 48 h, cell number was evaluated by direct counting. As shown in Fig. 2C, antibody addition induced an incomplete reduction of iron-dependent hyperproliferation, suggesting that iron capture by the cells employed only in part Tf/TfR. To confirm the possibility of a partial non-transferrin-mediated iron entry, we compared the effects on hBM-MSCs proliferation of FAC added for 3 days to a complete medium or to an FCS-lacking medium. As shown in Fig. 2D, although the effect of iron in the complete medium was stronger (due to the growth factors occurring in the serum), Fe was nevertheless capable of stimulating the cell growth when added to the serum-free medium. This suggests that iron might enter hBM-MSCs also by a transferrin-independent mechanism.

To investigate the possibility that iron affects cell proliferation by altering the distribution of cells in a specific cell cycle phase, we characterized, by FACS analysis, iron-treated (50 and 100 μM) hBM-MSCs compared to control cells. The cytofluorimetric investigation revealed a higher percentage of cells in S phase, indicating an increased rate of cell division (Fig. 3A). Conversely, no accumulation of cell debris (DNA content <2 N) was detected, suggesting the absence of iron-induced cellular toxic effects. This conclusion was further confirmed in cells exposed to increasing iron concentrations, based on the results of western blotting evaluation of procaspase 3 cellular contents (Fig. 3B). Procaspase 3 cleavage (and reduction) is in fact a marker of apoptotic activation. Further evidence of the iron promoting effect on cell proliferation was obtained from the analysis of regulatory components of the cell division cycle, namely cyclins and cyclin-dependent kinase inhibitors (CKIs). hBM-MSCs were treated for 48 h with different FAC concentrations, then nuclear and cytosolic extracts were prepared and assayed for various proteins involved in cell cycle regulation. As shown in Figs. 3C and 3D, iron induced the nuclear up-regulation of cyclin E and, more significantly, of cyclin A. Intriguingly, the analysis of the CKIs belonging to the Cip/Kip family showed a significant decrease of $p27^{Kip1}$ (Figs. 3C and 3D), even at low iron concentrations. No remarkable change in $p21^{Cip1}$ was observed, and we were unable to detect $p57^{Kip2}$ in hBM-MSCs (*data not reported*). We also analyzed the iron effects on MAPK pathway modulation. As shown in Fig. 4A, Fe^{3+} treatment increased phosphorylation of nuclear Erk1/2,
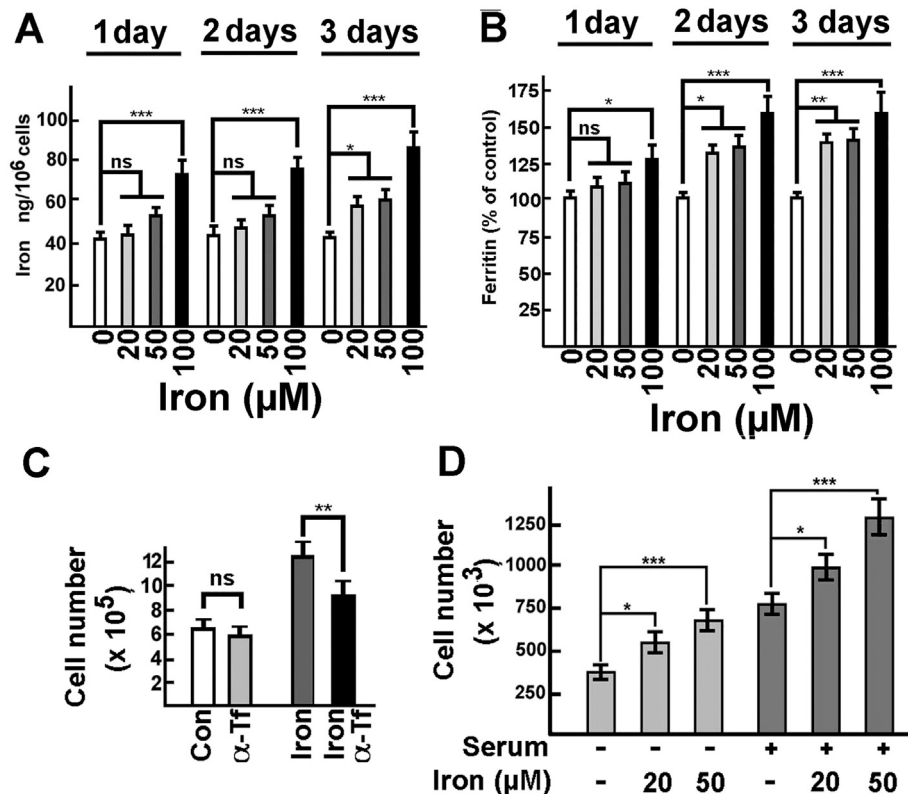

Fig. 2. Effect of iron treatment on hBM-MSC intracellular iron and ferritin content. Panel *A*: The total intracellular content of iron was evaluated in hBM-MSCs exposed for different time intervals to various iron concentrations. The data reported represent the mean values ± S.D. of three independent experiments; each experiment was performed in duplicate. ns, not significant, *P < 0.05 and ***P < 0.001 compared to 0 μM iron. Panel *B*: The total intracellular content of ferritin was evaluated in hBM-MSCs exposed for different time intervals to various iron concentrations. The data reported represent the mean values ± S.D. of three independent experiments; each experiment was performed in duplicate. ns, not significant, *P < 0.05, **P < 0.01, and ***P < 0.001 compared to 0 μM iron. Panel *C*: hBM-MSCs were grown without (Con) or with 100 μM iron added to 5% FCS culture medium. A total of 100 μg of rabbit anti-transferrin polyclonal antibodies (sc-21011, H-65, Santa Cruz Biotechnology) were added to the medium of both control and iron-treated cells. After 48 h, cell number was evaluated by direct counting. ns, not significant, **P < 0.01 compared to cell grown without antibodies added to the serum. Panel *D*: hBM-MSCs were grown for 3 days in SM or serum-free medium with or without different amount of iron. Then, cell number was evaluated by direct counting. The data reported represent the mean values ± S.D. of three independent experiments; each experiment was performed in duplicate. *P < 0.05 and ***P < 0.001 compared to 0 μM iron.
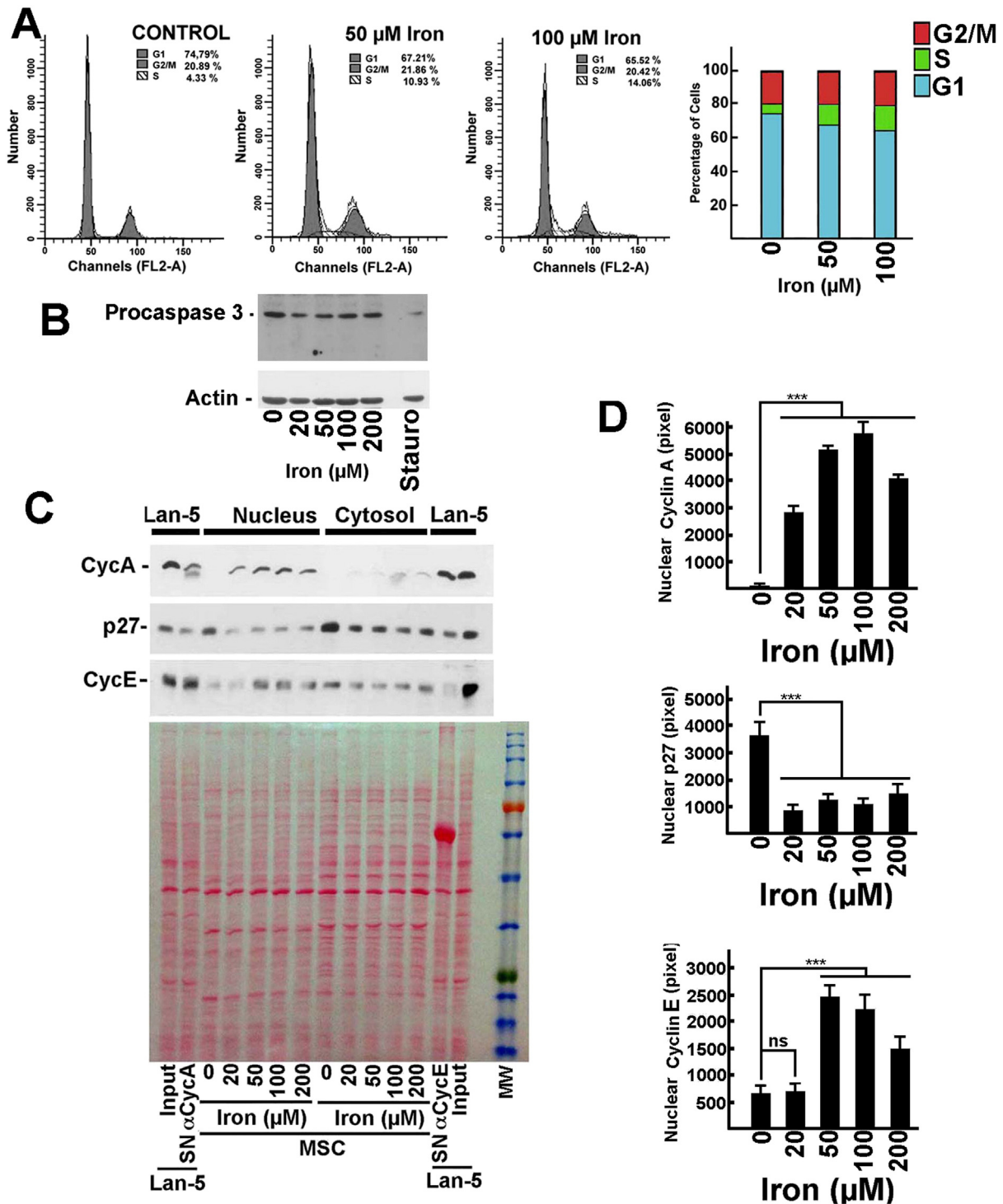
Fig. 3. Molecular effects of iron on cell proliferation parameters. Panel *A*: FACS analysis of hBM-MSCs grown for 48 h without (control) or with 50 μM and 100 μM iron. The data reported in the histogram (on the right) represent the mean of three independent experiments; each experiment was performed in duplicate. Panel *B*: hBM-MSCs were cultured for 48 h without or with different amounts of iron. Cells treated with staurosporin for 12 h were employed as positive control for apoptosis. Then, total cell extracts were prepared and 50 μg protein analyzed by immunoblotting using anti-procaspase and anti-actin antibodies. Panel *C*: hBM-MSCs were cultured for 48 h without or with different amounts of iron. Then, nuclear and cytosolic extracts were prepared. Equal amounts of proteins were analyzed by immunoblotting for the content of cyclin A, p27^{Kip1}, and cyclin E. Extracts of Lan-5 cells (a neuroblastoma cell line) were depleted of cyclin A or cyclin E. The input Lan-5 cell extracts and Lan-5 extracts supernatant after removal of cyclin A (SNαCycA) or cyclin E (SNαCycE) were analyzed to confirm the specificity of cyclin A and E signals. The panel also shows the filter stained with Ponceau S Red dye before immunoblotting for confirming equal loading. Panel *D*: The data reported in the histograms represent the mean of three independent experiments as those reported in the previous panel (i.e Fig. 3C) and quantified for cyclin A, p27, and cyclin E specific signals. Each experiment was performed in duplicate. ns, not significant, ***$P < 0.001$ compared to samples without iron.

suggesting that one of the effector mechanisms of iron might involve the up-regulation of this transduction pathway. A reasonable mechanism of iron-dependent growth stimulation activity is the increase in levels of ROS through the well-known Fenton's reaction, in which ferrous iron donates an electron in a reaction with hydrogen peroxide to produce the hydroxyl radical, a ROS [33]. Thus, the possibility that iron
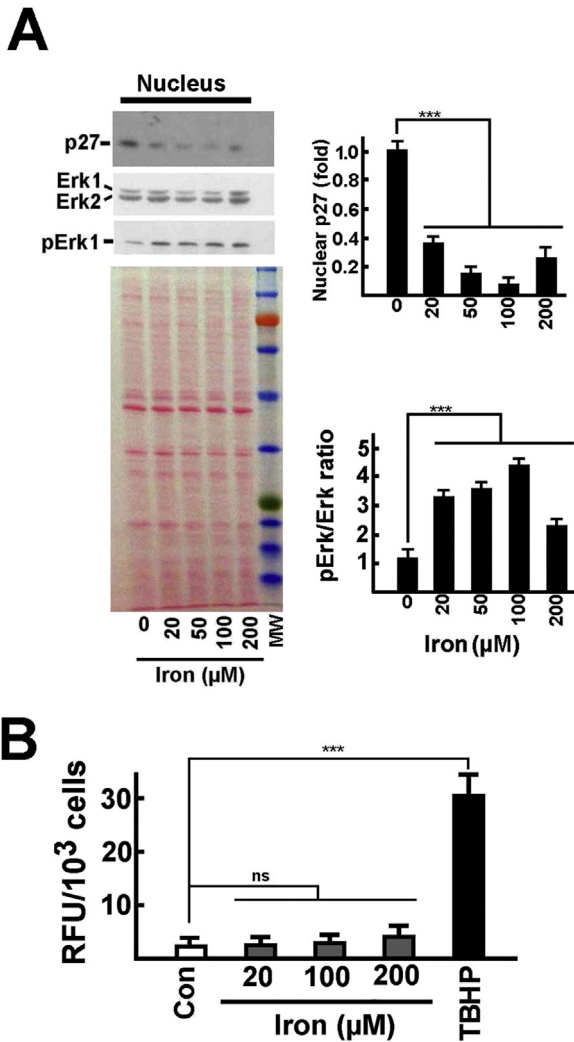
Fig. 4. Effects of iron treatment on Erk1/2 phosphorylation and intracellular ROS levels in hBM-MSCs. Panel *A*: hBM-MSCs were cultured for 48 h without or with different amounts of iron. Then, nuclear extracts were prepared. Equal amounts of proteins were analyzed by immunoblotting for the nuclear content of p27[Kip1], Erk1/2, and phosphoErk1/2 (pErk1/2). The panel also reports the filter stained with Red Ponceau before immunoblotting for confirming equal loading. The data reported in the histograms represent the mean of three independent experiments and are calculated on the basis of the pixel content of each analyzed signals. Pixels were obtained from the scanner of blots analyzed by ImageJ64 software. [***]*P* < 0.001 compared to 0 μM iron. Panel *B*: hBM-MSCs were grown without iron (Con) or with iron (at the indicated concentrations) and with 1 mM tert-butyl hydroperoxide (TBHP) for 3 h. Then ROS content was estimated using the 2′,7′-dichlorofluorescein diacetate method as reported in the Materials and methods section. The data reported represent the mean values ± S.D. of three independent experiments; each experiment was performed in duplicate. Con, untreated cells. [***]*P* < 0.001 compared to Con.

treatment caused an increase in ROS production was investigated. Because a change in ROS should occur rapidly after iron treatment, we used the DCF method to determine ROS levels after 3 h of treatment. Cells exposed to *ter*-butyl hydroxylperoxide were employed as positive control. At concentrations up to 100 μM FAC, no changes in cellular ROS levels were observed. At 200 μM, about 2-fold ROS accumulation occurred. Conversely, *ter*-butyl hydroxylperoxide elevated ROS by about 10-fold (Fig. 4B). Similar results were also obtained after 24 h of treatment (*data not reported*). Overall, our data demonstrate that iron stimulates the growth of hBM-MSCs in a concentration-dependent fashion. Iron entry occurs by transferrin-dependent and -independent mechanisms. The effect is not related to ROS production and it is associated to the accumulation of intracellular iron and ferritin. The proliferative

stimulation causes an increase in growth-associated cyclins (cyclin E and A) and the down-regulation of one CKI, p27[Kip1]. p21[Cip1] and p57[Kip2], the other two Cip/Kip CKIs, were not modulated.

3.2. Effect of iron overload on MSCs differentiation and matrix calcification

Frequently, the enhancement of proliferation is associated with a reduction of cell differentiation. Thus, we hypothesized that iron-dependent growth stimulation might affect the osteoblastic commitment of hBM-MSCs. Accordingly, we investigated whether accumulation of intracellular iron might influence the matrix calcification. Therefore, we first induced intracellular iron build-up and then activated osteogenic differentiation. Specifically, we treated confluent hBM-MSC cultures for 7 days with SM plus 100 μM FAC or SAC (as control). Thereafter, cells were washed with fresh medium and left for 1 day in SM (without iron). Finally, osteogenic medium (OM) was added to the cells for 2 weeks (as detailed in the scheme of Fig. 5A). In this experiment, we also tested the possible effect of vitamin C, because this molecule is an OM-component (see Materials and methods) and might affect iron activity. After OM incubation, we evaluated the extent of mineral calcification either by direct staining (Von Kossa method) or by determining the amount of calcium deposition. As shown in Fig. 5B, iron overloading (with or without vitamin C) caused a remarkable decrease in von Kossa staining of cell layers. The finding was confirmed by the levels of calcium detected in the matrix of OM-treated cells (Fig. 5C). Both these experiments indicate that iron overload strongly affects the *in vitro* calcification process. Figs. 5D and 5E reported the intracellular levels of iron and ferritin evaluated after the osteogenic differentiation (as reported in the scheme in Fig. 5A). As shown, vitamin C addition to the iron overloading-medium increased intracellular iron/ferritin deposition. The effect of iron on matrix calcification might be explained by different mechanisms, including i) an interference of iron with hydroxyapatite crystal formation, ii) an effect of iron on the osteoblastic commitment of hBM-MSCs, and iii) both mechanisms. To investigate these possibilities, we assessed the level of iron in the matrix after iron cell treatment and OM exposure. We identified a remarkable iron accumulation in the extracellular materials of iron-treated samples. As matter of facts, the iron content in the matrix of untreated cells was about 90 ± 11 ng/10^6 cells, while in the matrix of cells cultured in a medium added with 100 μM iron was 2.5 ± 0.5 μg/10^6 cells (both the values are the average ± S.D. of four independent experiments performed in duplicate). Thus, it is possible that iron directly competes with calcium for hydroxyapatite synthesis. It is also conceivable that iron might alter the synthesis and maturation of type I collagen. Therefore, type I collagen was extracted from the cell layers after iron overloading and compared with the amount of type I collagen produced by the same number of cells in the absence of Fe^{3+}. Amount of type I collagen was estimated by immunoblotting. In a preliminary experiment, we evaluated the relevance of vitamin C for type I collagen production. As shown in Fig. 6A, the amount of extractable type I collagen was higher in the presence of vitamin C. However, independently of the presence of L-ascorbic acid, iron strongly decreased type I collagen production. Since the procedure of collagen extraction from the matrix requires a prolonged pepsin treatment, no internal protein loading control could be used. However, in all the experiments, we analyzed cell layers containing an identical number of cells (1×10^6 cells). To validate the inhibitory effect of iron on collagen released in the matrix, we analyzed four distinct cell populations (Fig. 6B). In all cases, the negative effect of iron was confirmed. Because the reduced levels of collagen in iron-exposed hBM-MSC cultures might result from either down-regulation of type I collagen gene (COL1A1) transcription or altered maturation of the protein, we evaluated the effect of iron overload on COL1A1 gene transcript by RT-PCR. The electrophoretic separation of RT-PCR products, reported in Fig. 6C, clearly indicated that iron reduced COL1A1 gene expression. The decrease of COL1A1 gene transcription was also quantitatively evaluated by means of quantitative PCR as
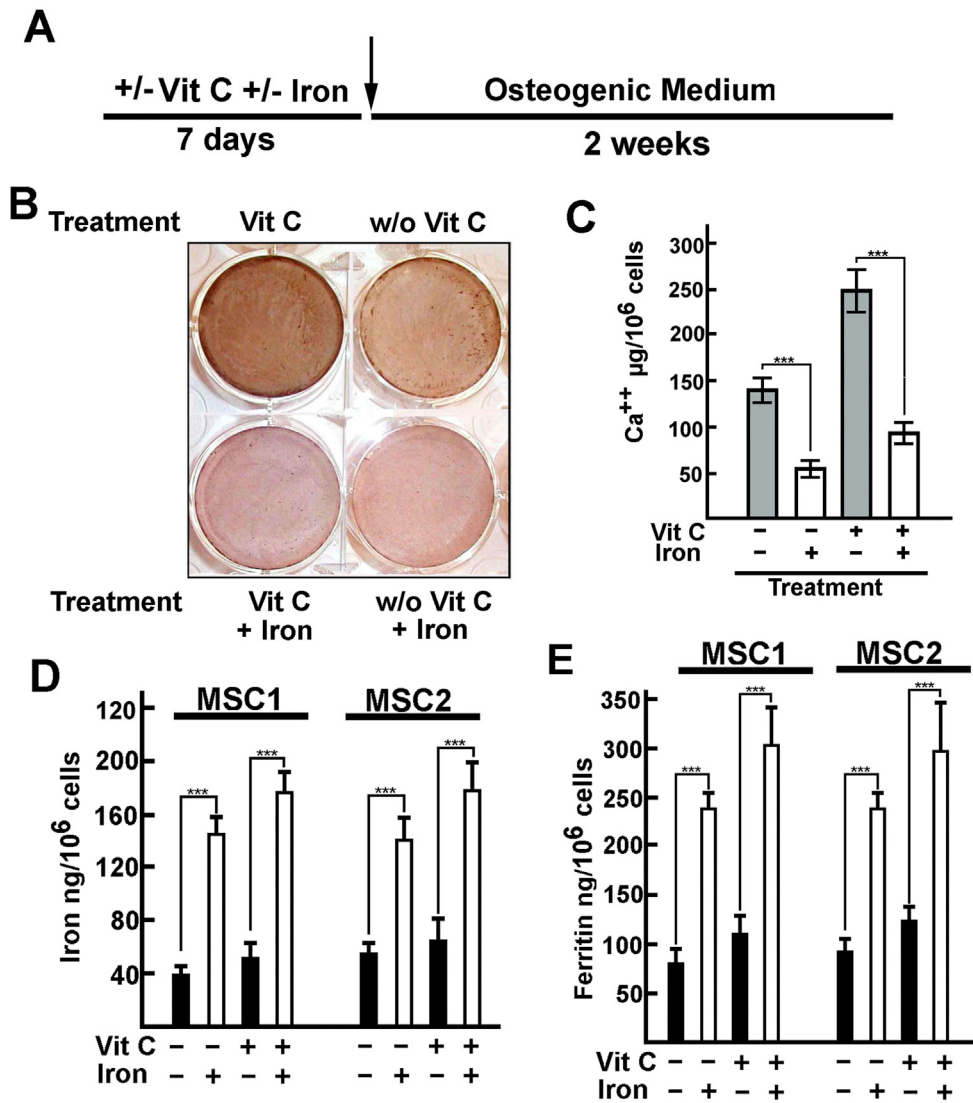
Fig. 5. Effect of iron on the matrix calcification. Panel *A*: The scheme summarizes the treatment employed in the subsequent panels. Panel *B*: hBM-MSCs were plated at high density and after reaching confluence were treated as reported. Iron concentration was 100 μM. Thereafter, the medium was substituted with OM (osteogenic medium) and after 2 further weeks the wells were stained with von Kossa staining. Panel *C*: hBM-MSCs were treated as in panel *A* and *B*. At the end of the experiment, calcium in the matrix was determined by the *o*-cresolphthalein complexone method as reported in the Materials and methods section. The data reported represent the mean values ± S.D. of two independent experiments; each experiment was performed in duplicate. ***$P < 0.001$ compared to samples without iron. Panel *D*: Histograms of intracellular hBM-MSC iron content of two different cell populations (named MSC1 and MSC2) after different iron-loading schemes. The data reported represent the mean values ± S.D. of three independent experiments; each experiment was performed in duplicate. ***$P < 0.001$ compared to samples without iron. Panel *E*: Histograms of intracellular hBM-MSC ferritin content of two different cell populations (defined MSC1 and MSC2) after different iron-loading schemes. The data reported represent the mean values ± S.D. of three independent experiments; each experiment was performed in duplicate. ***$P < 0.001$ compared to samples without iron.

reported in Fig. 6D. A key property of the osteoblastic phenotype is the vitamin D3-dependent expression of the osteocalcin gene and the subsequent extracellular release of the mature protein. This capability is not shown by other cells, including MSCs, and is considered a marker of osteoblastic commitment. As reported in Fig. 7A, a significant decrease of the osteocalcin production was observed in cells cultured for 72 h in the presence of 100 μM iron and the active form of vitamin D3. The finding argues for the view that iron alters hBM-MSC phenotypic commitment. We also investigated the levels of AP, a precocious marker of osteoblastic differentiation. AP amount was evaluated in terms of enzymatic activity (Fig. 7B) and protein levels (Fig. 7C). Both approaches demonstrated that AP was only slightly enhanced by iron treatment. Taken together, the results of our experiments suggest that Fe^{3+} overload alters the calcification process at different levels including collagen production and osteoblastic commitment. In addition,

iron accumulation could be detected in the calcified matrix, suggesting that iron overload might directly affect calcium deposition.

3.3. Effect of iron overload on gene expression

Iron is essential for the activity of several enzymes and thus changes in intracellular iron might affect numerous enzymatic reactions, both quantitatively and qualitatively. Among the iron-dependent enzymes, the so-called prolyl hydroxylases (PHDs) and asparaginyl hydroxylase (FIH) are of particular interest because they modulate the cellular content of hypoxia inducible factor (HIF)-alpha, a pivotal transcription factor involved in pO2-sensing mechanisms [34,35]. Poly(rC)-binding protein 1 (PCBP1), a key intracellular iron-delivering protein, can distribute iron to PHDs, thus allowing these enzymes to modulate levels of HIF proteins [36].
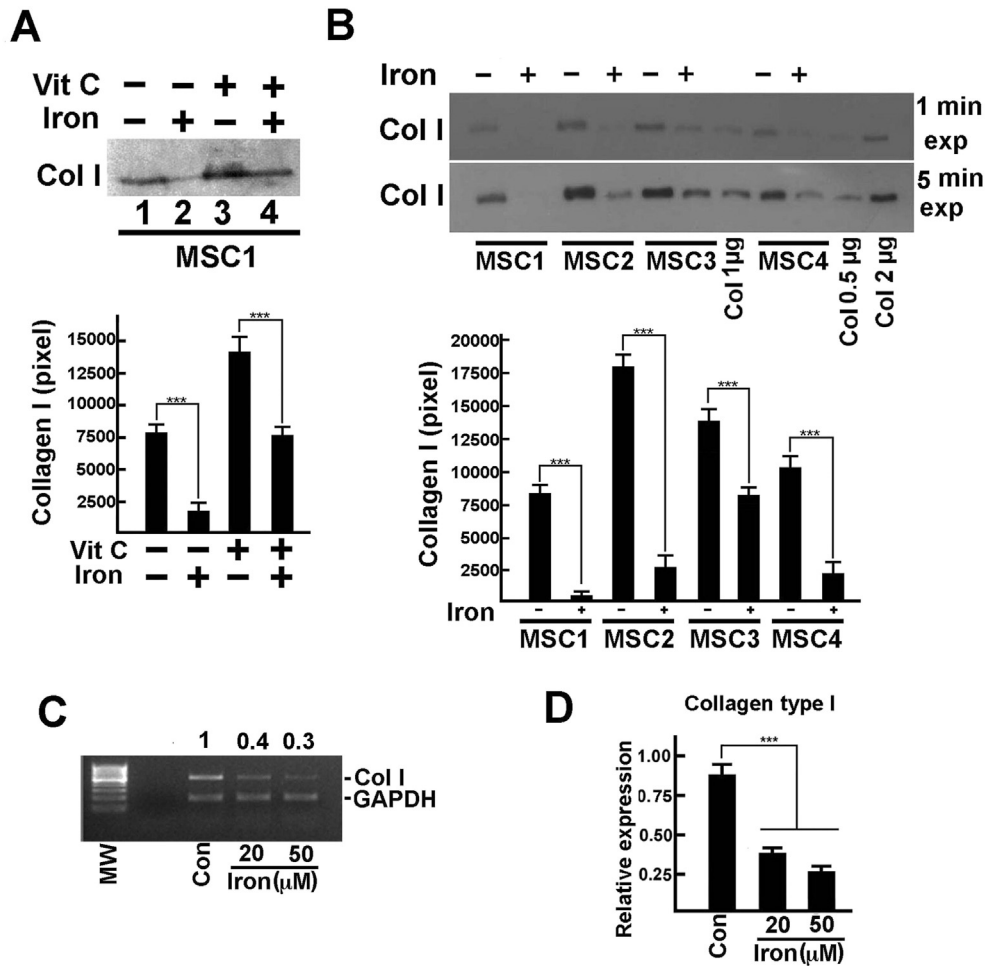
Fig. 6. Effect of iron on hBM-MSCs osteoblastic differentiation. Panel *A*: hBM-MSCs were cultured and treated as in Fig. 5A and 5B. The collagen was extracted from cell layers (see Materials and methods) containing equal number of cells and analyzed by immunoblotting for type I collagen content (Col I). Iron concentration used in this experiment was 100 μM. Three identical experiments (employing different cell preparations) were performed and the relative films were scanned and analyzed by ImageJ64 software. The data (pixels) reported in the histogram at the bottom represent the mean values ± S.D. ***$P < 0.001$ compared to samples without iron. Panel *B*: As in panel *A* except that vitamin C was used in all experiments and several independent hBM-MSC preparations were analyzed. Different amounts of collagen I protein standard were employed as internal standard. Two different exposition times were shown. Three identical experiments were performed and the relative films were scanned and analyzed by ImageJ64 software. The data reported (pixels) in the histogram at the bottom represent the mean values ± S.D. ***$P < 0.001$ compared to samples without iron. Panel *C*: hBM-MSCs were cultured and treated with different amounts of iron as in Fig. 5A and 5B. Then, RNA was extracted and the expression of *COL1A1* was evaluated by RT-PCR. *Glyceraldehyde-3-phosphate dehydrogenase* (*GAPDH*) was co-analyzed as internal standard. Additional experimental details are reported in the Materials and methods section. Panel *D*: Quantitative PCR analyses were performed to evaluate the effect of iron on *COL1A1* expression. Four identical experiments were performed. The data reported (as percentage of control) represent the mean values ± S.D. ***$P < 0.001$ compared to samples without iron (Con).

We hypothesized that an intracellular iron increase might result in the enhancement of PHD activity and thus in elevated prolyl hydroxylation->ubiquitination->degradation of HIF. To verify this hypothesis, we initially tried to estimate HIF levels by direct immunoblotting, but we failed to detect the protein in untreated or treated cells. Subsequently, for evaluating HIF-alpha modulation, the transcription of the genes controlled by HIF was determined.

Using a specific hypoxia signaling pathway RT-PCR array, we tested the effect of iron treatment (100 μM iron for 72 h) of hBM-MSCs on gene expression. We observed a significant transcriptional down-regulation effect (more than 2.5-fold) on a small number of genes, but none of the evaluated genes showed increased expression (Fig. 8A, *left panel*). The down-regulated genes identified were *endothelin 1*, *carbonic anhydrase 9*, *TfR1*, *angiopoietin-like protein 4*, and *coagulation factor 10*. Since these genes are regulated by several mechanisms including HIF level [36–43], we decided to compare these results with those of an experiment in which hBM-MSCs were treated to up-regulate HIF. Thus, cells were exposed to cobalt chloride, an inhibitor of PHDs [44]. As shown in Fig. 8A (*right*), several genes were up- and down-regulated

showing a pattern of modulation clearly in accord with HIF-alpha increase. However, with the exception of *coagulation factor 10*, the genes modulated by cobalt treatment were completely distinct from those regulated by iron addition.

The array data obtained by iron treatment were confirmed by real-time PCR experiments (Fig. 8B). The results reported suggest that iron might modulate gene expression, although a more detailed investigation appears necessary to fully characterize the pattern of iron effect on transcription. Moreover, our findings did not argue in favor of the view that iron overload might cause HIF-alpha modulation in hBM-MSCs.

4. Discussion

Iron overload syndromes include a broad range of hereditary and acquired conditions that have in common an excessive increase in total body iron stores. Abnormally elevated iron levels in the circulation cause Fe accumulation in several tissues and organs leading to hepatic disease, cardiac dysfunction, arthropathy, gonadal insufficiency, and
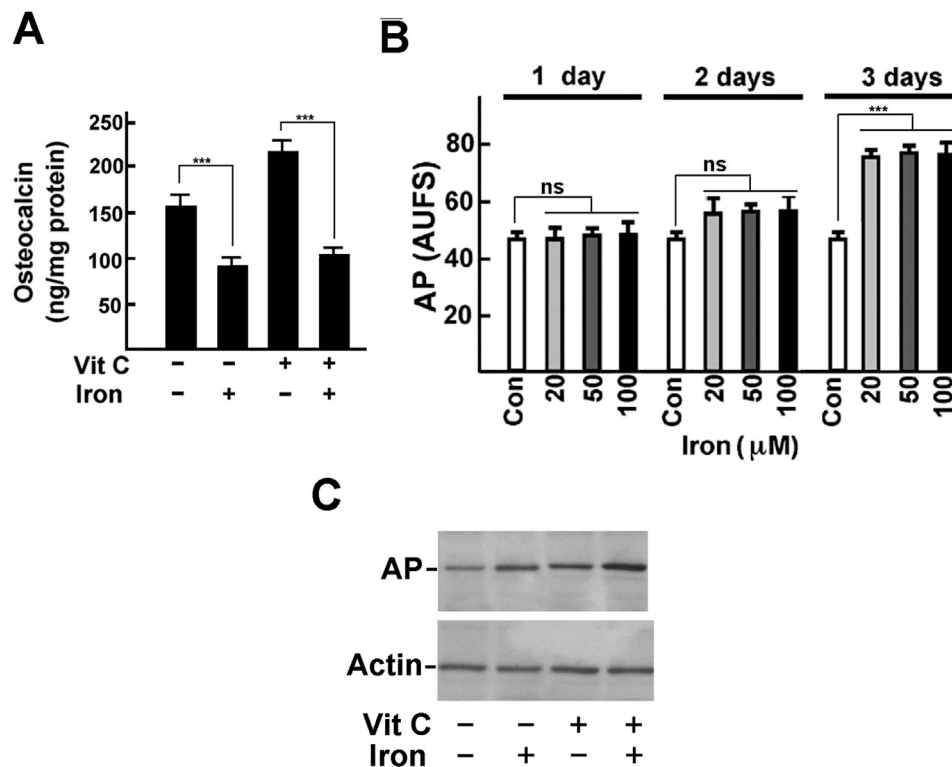
Fig. 7. Panel *A*: Confluent hBM-MSC cells were cultured for 2 weeks as indicated. Then, the cells were incubated in FCS-free Opti-MEM in the presence of 0.1% bovine serum albumin and 100 nM 1,25-dihydroxycholecalciferol for 48 h. Finally, osteocalcin level in the medium was determined. Further details are reported in the Materials and methods section. The data reported represent the mean values ± S.D. of three independent experiments; each experiment was performed in duplicate. ***P < 0.001 compared to sample without iron. Panel *B*: Intracellular alkaline phosphatase (AP) activity was determined in extracts of hBM-MSCs grown as indicated. The method for determining the enzyme activity was described under Materials and methods. The data reported represent the mean values ± S.D. of three independent experiments; each experiment was performed in duplicate. ns, not significant, ***P < 0.001 compared to sample without iron. Panel *C*: AP protein levels were determined in extracts of hBM-MSCs grown as described in panel *A*. The protein levels were evaluated by immunoblotting. Actin content was analyzed to verify equal protein loading. The image is representative of three independent experiments.

other endocrine disorders [1–5]. Fractures and osteoporosis also occur frequently in iron overload diseases, such as thalassemias [45] and hereditary hemochromatosis. It is unclear whether the mineral tissue alterations arise from a direct effect of iron on bone or might be the result of endocrine disorders (like hypogonadism), inefficacious erythropoiesis, or other negative conditions that can alter bone metabolism [7,46,47]. *In vitro* and animal data support the idea that iron excess directly controls bone mineral formation and/or remodeling [11,48]. Furthermore, a negative effect of iron overload has been reported on erythropoiesis [15]. No definitive explanations for such activities have been proposed, although ROS increase and apoptotic activation have been suggested as direct causes.

Taking these premises into consideration, we sought to shed light on how iron affects the growth and commitment of the physiological precursors of osteoblasts, namely hBM-MSCs. Of interest, these cells participate in the formation of the hemopoietic niche and thus play a key role in the overall process of hematopoiesis. Few and controversial data are so far available on the iron effect on primary cultures of mesenchymal cells [24–27,49].

The results of our study provide evidence that hBM-MSCs accumulate intracellular iron and thus represent a target of iron overload. In addition, we demonstrate in hBM-MSCs at early passages (2nd–3rd passages) that the metal induces growth stimulation, alters gene expression, decreases formation of type I collagen, and, finally, reduces hydroxyapatite formation and matrix calcification.

Iron concentrations used in our experiments (20–200 μM) ranged from serum physiological concentrations to levels identified in overloaded subjects. We avoided using iron amounts higher than 200 μM since these concentrations are not generally reached in patients. Iron was added as FAC, which has been reported to mimic NTBI, Non-

Transferrin Bound Iron form, found up-regulated in the plasma of iron overloaded patients [32]. Since SM, the medium used to culture hBM-MSCs, includes 10% FCS, and FCS contains about 2 mg/ml of transferrin with a high degree of saturation (50–90%) and about 1 μg/ml of iron bound to serum ferritin [50], we considered that iron occurring in our SM was almost totally bound to transferrin and that our SM might have a residual iron binding capability (due to transferrin) of about 0.3–2.5 nmoles/ml. This scarce binding efficiency suggests that FAC added to SM remains essentially as NBTI.

However, the ultrafiltration analysis of Fe occurring in SM, added or not with 20–100 μM FAC, demonstrated that more than 90% of iron is bound to material with a molecular weight higher than 10 KDa (*data not reported*). This is in accord with data on NTBI in plasma of iron overloaded patients indicating that NTBI is mostly associated to plasma proteins [51]. So far, the characterization of iron species in plasma NTBI has not been conclusive, mainly because of the very heterogenic nature and composition of NTBI itself, which might vary in different pathologies. In systemic iron overload, NTBI has been reported as associated with various plasma components including organic acids like phosphates, citrate, and proteins. However, the analysis by size-filtration of plasma from thalassemic patients, or from non-chelated patients, show that the active forms of NTBI consist of high-molecular-weight complexes, most probably associated to proteins [51].

We observed a clear cellular uptake of iron in hBM-MSCs exposed to the metal. Fe accumulation was demonstrated by analyzing iron levels and was identified as statistically significant at 100 μM iron after 1 day of treatment and at 20 μM after 3 days. The increase of intracellular iron was definitely confirmed by ferritin up-regulation. As matter of facts, only intracellular iron might increase the translation of ferritin transcript, and thus ferritin level is a direct marker of cellular iron
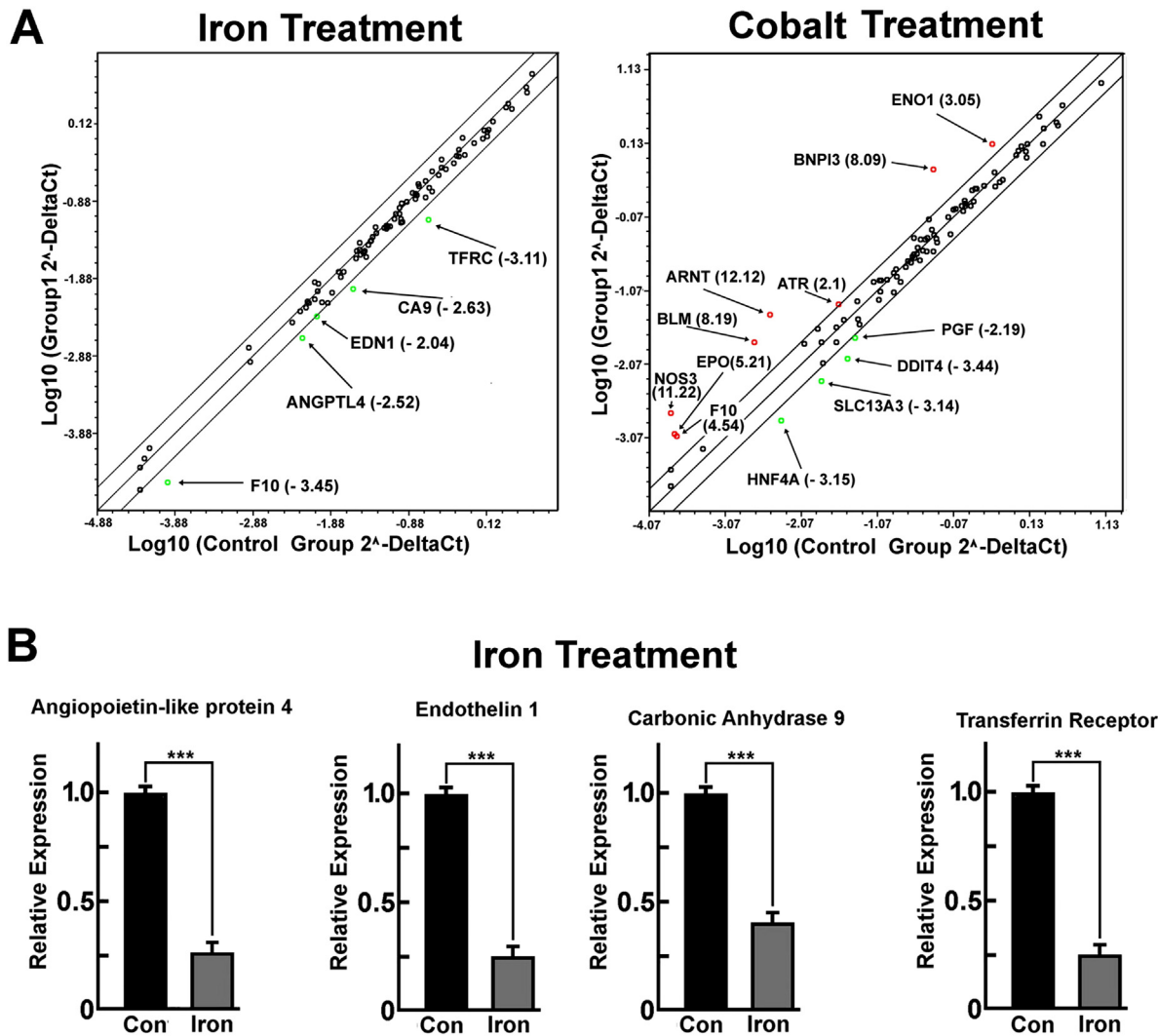
Fig. 8. Effect of iron on hBM-MSC gene expression. Panel *A. On the left*: proliferating hBM-MSCs were plated at low density and treated with FAC (100 μM) or SAC (100 μM) for 72 h. Total RNA was extracted from treated and control cells, using TRIzol reagent according to the manufacturer's instructions (Invitrogen) and resuspended in RNase-free water. After the preparation of cDNA, gene expression was evaluated by RT^2 Profiler PCR arrays specific for the Hypoxia Signaling Pathway (PAHS-032ZA-12). Only changes greater than 2.5 fold were reported. *On the right*: proliferating hBM-MSCs were plated at low density and treated with NaCl (200 μM) or CoCl$_2$ (100 μM) for 72 h. Then, the experiment was performed as in panel on the left. Panel *B*: The figure reports the results of qPCR independent experiments confirming the data obtained from the above reported array on iron treatment (Fig. 8A, left). Particularly, the data represent the mean values ± S.D. of three independent experiments; each experiment was performed in duplicate. Con, Control. ***$P < 0.001$ compared to sample without iron.

elevation. We concluded that extracellular increase of iron might cause accumulation of the metal in hBM-MSCs, suggesting that these cells could be thought of as iron reservoir and cellular targets in iron overload syndromes. Under our experimental conditions, the entry of iron seems mediated in part by transferrin and in part by a direct FAC uptake (Fig. 2). This is similar to findings reported in other cellular models [52–54].

When we evaluated the effect of iron on the proliferation rate, we found for the first time that iron clearly and strongly stimulated hBM-MSCs cell growth in a concentration-dependent manner. The effect was consistently demonstrated in all the cell preparations employed. No signs of apoptosis were identified up to 100 μM, as showed by FACS analysis (absence of a sub-G1 peak) and by the absence of procaspase 3 cleavage (Figs 3A and 3B).

The stimulation of growth was confirmed at molecular level through the analyses of cyclins and cyclin-dependent kinase inhibitors. The marked increase of cyclin E and cyclin A suggested an accelerated entry into S phase. This was directly confirmed by FACS analysis. Most interestingly, iron treatment caused a rapid decrease in p27^{Kip1},

which was evident at iron concentrations as low as 20 μM. No effect on p21^{Cip1} and p57^{Kip2} was observed, suggesting that p27Kip1 plays a peculiar and important role in hBM-MSCs proliferation control and confirming previous data [55]. We also investigated the bases of iron-dependent accelerated proliferation. One important finding is that the growth stimulation does not appear to be associated with ROS increase; in fact, we found no evidence, at least at the concentrations employed, that iron treatment increases ROS. Conversely, we observed the activation of MAPK pathway, which could be considered at least one cause of p27Kip1 decrease and accelerated growth. The elevated S phase entry is in agreement with several findings showing either a decrease of cells in S phase or the up-regulation of G1 phase cells upon treatment with iron chelating agents [56].

The iron-dependent hBM-MSC growth stimulation prompted us to investigate the effect of iron also on matrix calcification. *In vitro*, the treatment of hBM-MSCs with the so-called osteogenic medium induces their differentiation into osteoblasts and the deposition of type I collagen. Subsequently, the extracellular matrix undergoes calcification, as revealed by specific staining procedures and evaluation of

matrix calcium deposition. However, the entire calcification process is complex and involves numerous, contemporaneous, and not completely recognized steps. To identify the precise events affected by iron, we decided to preload hBM-MSCs with iron, wash the cells, and then add the OM.

The immunoblotting analysis of type I collagen demonstrated a strong reduction of this protein in the matrix of iron-preloaded cells. The down-regulation might be explained by the observed clear reduction of *COL1A1* transcription (as estimated by quantitative PCR). We cannot, however, exclude a negative effect of iron on collagen maturation, being the hydroxylation of collagen prolines and lysines subjected to iron-dependent regulation.

To investigate the effect of iron on the differentiation of hBM-MSCs into osteoblasts, we evaluated its activity on osteocalcin production. Osteocalcin gene expression occurs only in mature osteoblasts and not in hBM-MSCs. Thus, the decrease in osteocalcin released into the medium suggests that iron also alters the physiological differentiation of hBM-MSCs toward mature osteoblasts. Finally, when we evaluated the effect of iron on the calcification process *in toto*, we clearly identified the diminished formation of hydroxyapatite (it reduces calcium precipitation).

A further experiment demonstrating that iron modifies hBM-MSC phenotypic features was the gene expression array analysis of Fe-treated cells. Although this analysis takes into consideration only genes involved in hypoxia-related pathways, the findings suggested that iron is able to modulate specific gene expression. The choice of analyzing HIF-modulated genes is related to the role of iron-dependent reactions in HIF degradation [34,35]; furthermore, HIF-1α activity is induced by the mycobacterial Fe–chelator desferri–exochelin [57]. However, when we compared the effect of iron treatment with that of cobalt ion (a known HIF-alpha inducer), we did not find any gene modulated by both the molecules (with the exception of coagulation factor 10) (Fig. 8A). The finding suggests that the effect of iron on

gene expression is not (or scarcely) mediated by the control of HIF level, at least in BM-MSCs. Thus, while it clearly appears that iron might control the level and activity of specific transcripts, their identification and correlation with specific iron-modulated cellular mechanisms need further investigations.

In summary, the reported data indicate that iron affects both osteoblastic phenotypic features and mature hydroxyapatite formation (Fig. 9). These observations might explain the molecular bases of bone alterations, mostly osteoporosis and fractures, occurring in iron overload syndromes. As matter of facts, the increase of iron-dependent proliferation of BM-MSCs associated to a reduction of differentiation and correct matrix calcification might account, at least in part, not only for low bone mineral density, but also for the hemopoietic niche defects and the severe hematopoietic dysfunctions, frequently reported in iron overload syndromes.

Author contributions

F.D.R., A.B., and S.P. contributed to the conception and design of the study and the interpretation of the data, and drafted the manuscript; A.O., B.N., and F.L. contributed to the design of the study and drafted, reviewed, and approved the manuscript; F.D.R. and A.B. contributed to the design of the experiments based on cell cultures and protein analyses, acquisition of the images, and prepared the figures; I.C., M.C.S., and D.B. performed biochemical and immunochemical studies on primary cultures of MSCs; S.S. and S.P. contributed to the design and accomplishment of the expression array experiments; I.C. and A.T. contributed to the design and accomplishment of the experiments based on RT-PCR; A.B., I.C., and E.S. contributed to the design and accomplishment of the experiments on osteogenic differentiation of MSC including staining procedures; A.O., A.N., and A.B. contributed to the establishing and characterization of MSCs.

Transparency document

The Transparency document associated with this article can be found, in the online version.

Acknowledgments

Fig. 9. Schematic representation of iron effect on mesenchymal stromal cells. The scheme summarizes the data obtained in the present study. Iron, at concentrations occurring in the serum of iron overloaded patients, stimulates hBM-MSC proliferation and self-renewal by increasing the levels of cyclin A and cyclin E and MAPK pathway activity. Contemporaneously, the metal decreases the intracellular content of p27^{Kip1} (p27), a cyclin-dependent kinase inhibitor. Additionally, iron affects hBM-MSCs differentiation by decreasing the synthesis and maturation of type I collagen I (Col I). Finally, matrix calcification is further modified by the accumulation of iron and the decrease of calcium content.

References

[1] A. Piperno, Classification and diagnosis of iron overload, Hematologica 83 (1998) 447–455.

[2] R.E. Fleming, P. Ponka, Iron overload in human disease, N. Engl. J. Med. 366 (2012) 348–359.

[3] P.C. Adams, J.C. Barton, Haemochromatosis, Lancet 370 (2007) 1855–1860.

[4] A. Pietrangelo, Hereditary hemochromatosis: pathogenesis, diagnosis, and treatment, Gastroenterology 139 (2010) 393–408.

[5] A. Siddique, K.V. Kowdley, The iron overload syndromes, Aliment. Pharmacol. Ther. 35 (2012) 876–893.

[6] C.P. Ozment, J.L. Turi, Iron overload following red blood cell transfusion and its impact on disease severity, Biochim. Biophys. Acta 2009 (1790) 694–701.

[7] P. Guggenbuhl, Y. Deugnier, J.F. Boisdet, et al., Bone mineral density in men with genetic hemochromatosis and HFE gene mutation, Osteoporos. Int. 16 (2005) 1809–1814.

[8] M. Sarrai, H. Duroseau, J. D'Augustine, et al., Bone mass density in adults with sickle cell disease, Br. J. Hematol. 136 (2007) 666–672.

[9] L. Valenti, M. Varenna, A.L. Fracanzani, et al., Association between iron overload and osteoporosis in patients with hereditary hemochromatosis, Osteoporos. Int. 20 (2009) 549–555.

[10] N. Skordis, M. Toumba, Bone disease in thalassemia major: recent advances in pathogenesis and clinical aspects, Pediatr. Endocrinol. Rev. 8 (Suppl. 2) (2011) 300–306.
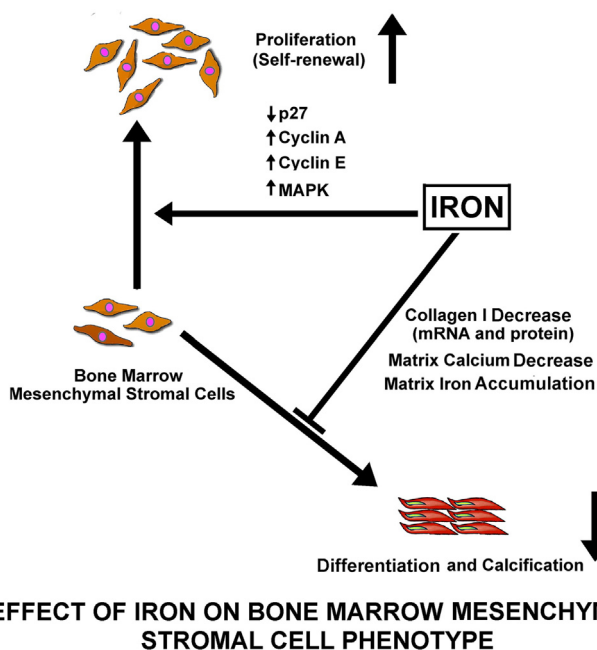
[11] H. Isomura, K. Fujie, K,.I. Shibata, et al., Bone metabolism and oxidative stress in postmenopausal rats with iron overload, Toxicology 197 (2004) 93–100.

[12] J. Tsay, Z. Yang, F.P. Ross, et al., Bone loss caused by iron overload in a murine model: importance of oxidative stress, Blood 116 (2010) 2582–2589.

[13] E.N. Oliva, F. Ronco, A. Marino, et al., Iron chelation therapy associated with improvement of hematopoiesis in transfusion-dependent patients, Transfusion 50 (2010) 1568–1570.

[14] M.A. Badawi, L.M. Vickars, J.M. Chase, H.A. Leitch, Red blood cell transfusion independence following the initiation of iron chelation therapy in myelodysplastic syndrome, Adv. Hematol. 2010 (2010) 164045.

[15] K. Taoka, K. Kumano, F. Nakamura, et al., The effect of iron overload and chelation on erythroid differentiation, Int. J. Hematol. 95 (2012) 149–159.

[16] M.F. Pittenger, A.M. Mackay, S.C. Beck, et al., Multilineage potential of adult human mesenchymal stem cells, Science 284 (1999) 143–147.

[17] P.A. Zuk, M. Zhu, P. Ashjian, et al., Human adipose tissue is a source of multipotent stem cells, Mol. Biol. Cell 13 (2002) 4279–4295.

[18] S.A. Wexler, C. Donaldson, P. Denning-Kendall, et al., Adult bone marrow is a rich source of human mesenchymal 'stem' cells but umbilical cord and mobilized adult blood are not, Br. J. Hematol. 121 (2003) 368–374.

[19] M. Al-Nbaheen, R. Vishnubalaji, D. Ali, et al., Human stromal (mesenchymal) stem cells from bone marrow, adipose tissue and skin exhibit differences in molecular phenotype and differentiation potential, Stem Cell Rev. 91 (2013) 32–43.

[20] S.P. Bruder, D.J. Fink, A.I. Caplan, Mesenchymal stem cells in bone development, bone repair, and skeletal regeneration therapy, J. Cell. Biochem. 56 (1994) 283–294.

[21] F. Dazzi, R. Ramasamy, S. Glennie, et al., The role of mesenchymal stem cells in hemopoiesis, Blood Rev. 20 (2006) 161–171.

[22] S. Méndez-Ferrer, T.V. Michurina, F. Ferraro, et al., Mesenchymal and hematopoietic stem cells form a unique bone marrow niche, Nature 466 (2010) 829–834.

[23] M. Di Nicola, C. Carlo-Stella, M. Magni, et al., Human bone marrow stromal cells suppress T-lymphocyte proliferation induced by cellular or nonspecific mitogenic stimuli, Blood 99 (2002) 3838–3843.

[24] K. Yamasaki, H. Hagiwara, Excess iron inhibits osteoblast metabolism, Toxicol. Lett. 191 (2009) 211–215.

[25] J.G. Messer, A.K. Kilbarger, K.M. Erikson, D.E. Kipp, Iron overload alters iron-regulatory genes and proteins, down-regulates osteoblastic phenotype, and is associated with apoptosis in fetal rat calvaria cultures, Bone 45 (2009) 972–979.

[26] M. Doyard, N. Fatih, A. Monnier, et al., Iron excess limits HHIPL-2 gene expression and decreases osteoblastic activity in human MG-63 cells, Osteoporos. Int. 23 (2012) 2435–2445.

[27] G.Y. Zhao, L.P. Zhao, Y.F. He, et al., Comparison of the biological activities of human osteoblast hFOB1.19 between iron excess and iron deficiency, Biol. Trace Elem. Res. 150 (2012) 487–495.

[28] A. Oliva, I. Passaro, R. Di Pasquale, et al., Ex vivo expansion of bone marrow stromal cells by platelet-rich plasma: a promising strategy in maxillo-facial surgery, Int. J. Immunopathol. Pharmacol. 18 (2005) 47–53.

[29] A. Borriello, I. Caldarelli, M.A. Basile, et al., The tyrosine kinase inhibitor dasatinib induces a marked adipogenic differentiation of human multipotent mesenchymal stromal cells, PLoS One 6 (2011), e28555.

[30] S. Perrotta, N. Di Iorgi, F. Della Ragione, et al., Early-onset central diabetes insipidus is associated with de novo arginine vasopressin-neurophysin II or Wolfram syndrome 1 gene mutations, Eur. J. Endocrinol. 172 (2015) 461–472.

[31] A. Borriello, I. Caldarelli, D. Bencivenga, et al., p57Kip2 is a downstream effector of BCR-ABL kinase inhibitors in chronic myelogenous leukemia cells, Carcinogenesis 32 (2011) 10–18.

[32] Z.I. Cabantchik, Labile iron in cells and body fluids: physiology, pathology, and pharmacology, Front. Pharmacol. 5 (2014) 45, http://dx.doi.org/10.3389/fphar.2014.00045. eCollection 2014.

[33] P. Wardman, L.P. Candeias, Fenton chemistry: an introduction, Radiat. Res. 145 (1996) 523–531.

[34] R.K. Bruick, S.L. McKnight, A conserved family of prolyl-4-hydroxylases that modify HIF, Science 294 (2001) 1337–1340.

[35] J. Myllyharju, Prolyl 4-hydroxylases, master regulators of the hypoxia response, Acta Physiol. 208 (2013) 148–165.

[36] A. Nandal, J.C Ruiz, P. Subramanian, et al., Activation of the HIF prolyl hydroxylase by the iron chaperones PCBP1 and PCBP2, Cell Metab. 14 (2011) 647–657.

[37] S. Le Jan, C. Amy, A. Cazes, et al., Angiopoietin-like 4 is a proangiogenic factor produced during ischemia and in conventional renal cell carcinoma, Am. J. Pathol. 162 (2003) 1521–1528.

[38] S. Kaluz, M. Kaluzová, S.Y. Liao, et al., Transcriptional control of the tumor- and hypoxia-marker carbonic anhydrase 9: a one transcription factor (HIF-1) show? Biochim. Biophys. Acta 2009 (1795) 162–172.

[39] H. Li, C Ge, F. Zhao, et al., Hypoxia-inducible factor 1 alpha–activated angiopoietin-like protein 4 contributes to tumor metastasis via vascular cell adhesion molecule-1/integrin b1 signaling in human hepatocellular carcinoma, Hepatology 54 (2011) 910–919.

[40] P. Zhu, Y.Y. Goh, H.F.A. Chin, et al., Angiopoietin-like 4: a decade of research, Biosci. Rep. 32 (2012) 211–219.

[41] M.C. Ghosh, D.L. Zhang, S.Y. Jeong, et al., Deletion of iron regulatory protein 1 causes polycythemia and pulmonary hypertension in mice through translational derepression of HIF2α, Cell Metab. 17 (2013) 271–281.

[42] C. Zhang, Essential functions of iron-requiring proteins in DNA replication, repair and cell cycle control, Protein Cell 5 (2014) 750–760.

[43] S.V. Torti, F.M. Torti, Iron and cancer: more ore to be mined, Nat. Rev. Cancer 13 (2013) 342–355.

[44] P.H. Maxwell, M.S. Wiesener, G.W. Chang, et al., The tumour suppressor protein VHL targets hypoxia-inducible factors for oxygen-dependent proteolysis, Nature 399 (1999) 271–275.

[45] M.G. Vogiatzi, E.A. Macklin, E.B. Fung, et al., Prevalence of fractures among the thalassemia syndromes in North America, Bone 2038 (2006) 571–575.

[46] E.D. Weinberg, Role of iron in osteoporosis, Pediatr. Endocrinol. Rev. 6 (Suppl. 1) (2008) 81–85.

[47] M.G. Vogiatzi, E.A. Macklin, E.B. Fung, et al., Bone disease in thalassemia: a frequent and still unresolved problem, J. Bone Miner. Res. 24 (2009) 543–557.

[48] H. Kudo, S. Suzuki, A. Watanabe, et al., Effects of colloidal iron overload on renal and hepatic siderosis and the femur in male rats, Toxicology 246 (2008) 143–147.

[49] Y. Zhang, W. Zhai, M. Zhao, et al., Effects of iron overload on the bone marrow microenvironment in mice, PLoS One 10 (2015), e0120219.

[50] K. Kakuta, K. Orino, S. Yamamoto, K. Watanabe, High levels of ferritin and its iron in fetal bovine serum, Comp. Biochem. Physiol. A Physiol. 118 (1997) 165–169.

[51] R.W. Evans, R. Rafique, A. Zarea, et al., Nature of non-transferrin-bound iron: studies on iron citrate complexes and thalassemia sera, J. Biol. Inorg. Chem. 13 (2008) 57–74.

[52] Y.S. Sohn, H. Ghoti, W. Breuer, et al., The role of endocytic pathways in cellular uptake of plasma non-transferrin iron, Haematologica 97 (2012) 670–678.

[53] J. Arezes, M. Costa, I. Vieira, et al., Non-transferrin-bound iron (NTBI) uptake by T lymphocytes: evidence for the selective acquisition of oligomeric ferric citrate species, PLoS One 8 (2013), e79870.

[54] E. Pourcelot, M. Lénon, N. Mobilia, et al., Iron for proliferation of cell lines and hematopoietic progenitors: nailing down the intracellular functional iron concentration, Biochim. Biophys. Acta 2015 (1853) 1596–1605.

[55] Y. Yu, Z. Kovacevic, D.R. Richardson, Tuning cell cycle regulation with an iron key, Cell Cycle 6 (2007) 1982–1994.

[56] D.R. Richardson, Potential of iron chelators as effective antiproliferative agents, J. Physiol. Pharmacol. 75 (1997) 1164–1180.

[57] T.W. Chong, L.D. Horwitz, J.W. Moorem, et al., A mycobacterial iron chelator, desferri-exochelin, induces hypoxia-inducible factors 1 and 2, NIP3, and vascular endothelial growth factor in cancer cell lines, Cancer Res. 62 (2002) 6924–6927.